https://doi.org/10.5194/bg-2023-160
Preprint. Discussion started: 10 October 2023

Biogeosciences
Discussions
Open Access

Assessing improvements in global ocean pCO_2 machine learning reconstructions with Southern Ocean autonomous sampling

Thea H. Heimdal[1], Galen A. McKinley[1], Adrienne J. Sutton[2], Amanda R. Fay[1], Lucas Gloege[3]

[1]Columbia University and Lamont-Doherty Earth Observatory, Palisades, NY, USA

[2]Pacific Marine Environmental Laboratory, National Oceanic and Atmospheric Administration, Seattle, WA, USA

[3]Open Earth Foundation, Marina del Rey, CA, USA

Correspondence to: Thea H. Heimdal (theimdal@ldeo.columbia.edu)

Abstract

The Southern Ocean plays an important role in the exchange of carbon between the atmosphere and oceans, and is a critical region for the ocean uptake of anthropogenic CO_2. However, estimates of the Southern Ocean air-sea CO_2 flux are highly uncertain due to limited data coverage. Increased sampling in winter and across meridional gradients in the Southern Ocean may improve machine learning (ML) reconstructions of global surface ocean pCO_2. Here, we use a Large Ensemble Testbed (LET) of Earth System Models and the pCO_2-Residual reconstruction method to assess improvements in pCO_2 reconstruction fidelity that could be achieved with additional autonomous sampling in the Southern Ocean added to existing Surface Ocean CO_2 Atlas (SOCAT) observations. The LET allows us to robustly evaluate the skill of pCO_2 reconstructions in space and time through comparison to 'model truth'. With only SOCAT sampling, Southern Ocean and global pCO_2 are overestimated, and thus the ocean carbon sink is underestimated. Incorporating Uncrewed Surface Vehicle (USV) sampling increases the spatial and seasonal coverage of observations within the Southern Ocean, leading to a decrease in the overestimation of pCO_2. A modest number of additional observations in southern hemisphere winter and across meridional gradients in the Southern Ocean leads to improvement in reconstruction bias and root-mean squared error (RMSE) can be improved by as much as 65 % and 19 %, respectively, as compared to using SOCAT sampling alone. Lastly, the large decadal variability of air-sea CO_2 fluxes shown by SOCAT-only sampling, may be partially attributable to undersampling of the Southern Ocean.

https://doi.org/10.5194/bg-2023-160
Preprint. Discussion started: 10 October 2023

1. Introduction

The ocean plays an important role in mitigating against climate change by sequestering anthropogenic carbon emissions. Since 1850, the oceans have removed a total of 170 ± 35 Gt of carbon (Friedlingstein et al., 2022). In order to fully understand the climate impacts from rising emissions, it is essential to accurately quantify the air-sea CO_2 flux and the global ocean carbon sink in space and time. The Surface Ocean CO_2 ATlas (SOCAT; Bakker et al., 2016) is the largest global database of surface ocean CO_2. It contains over 33 million high-quality direct shipboard measurements of fCO_2 (uncertainty of < 5 µatm), which have been gathered since 1957 (Bakker et al., 2022). However, due to limited resources for ocean observing, limited number of ships/routes, inaccessible regions and unsafe waters, the database covers only about 1% of the global ocean at monthly 1°x1° spatial resolution over the period of 1982-2023, and is highly biased towards the northern hemisphere.

Observation-based data products have been developed to better constrain surface ocean pCO_2 in space and time by extrapolating to global coverage from the sparse SOCAT observations (e.g., Landschützer et al., 2014; Rödenbeck et al., 2015; Gloege et al., 2022; Bennington et al., 2022a,b). These data products utilize machine learning (ML) algorithms to estimate a non-linear function between a suite of driver variables (i.e., sea surface temperature; SST, sea surface salinity; SSS, mixed layer depth; MLD, Chlorophyll; Chl-a, xCO_2; atmospheric CO_2) and ocean pCO_2 (the target variable) where these are co-located. The driver variables are proxies for processes influencing ocean pCO_2. Full-coverage driver variable datasets are then processed through these ML algorithms to produce estimated global full-coverage surface ocean pCO_2. Since the data products rely on observations to train the algorithms and thus produce these relationships, data sparsity remains a fundamental limitation to this technique.

It has been suggested that targeted sampling from autonomous platforms combined with ships, filling in the state space of pCO_2, represent a likely path forward to improve surface ocean pCO_2 reconstructions (Bushinsky et al., 2019; Gregor et al., 2019; Gloege et al., 2021; Djeutchouang et al., 2022; Landschützer et al., 2023). One major obstacle, however, is that the indirect pCO_2 estimates from floats have high uncertainties (± 11.4 µatm) and may be biased by as much as ~ 4 µatm (Bakker et al., 2016; Williams et al., 2017; Fay et al., 2018; Gray et al., 2018; Sutton et al., 2021; Mackay and Watson 2021; Wu et al 2022). Biases and uncertainties can have

https://doi.org/10.5194/bg-2023-160
Preprint. Discussion started: 10 October 2023

large impacts on global air-sea CO_2 flux estimates, given that the global mean air-sea disequilibrium is only 5-8 µatm (McKinley et al., 2020). It is therefore critical that bias and uncertainty corrections are well-constrained over different oceanic conditions and over time.

Uncrewed Surface Vehicles (USVs), such as those manufactured and maintained by Saildrone Inc., represent a new type of autonomous platform that can obtain direct pCO_2 observations with significantly lower uncertainties compared to other autonomous methods, and equivalent to the highest-quality shipboard measurements contained in SOCAT (± 2 µatm; Sabine et al., 2020; Sutton et al., 2021). Such improvements in sampling are critically important in the undersampled Southern Ocean. This region is fundamental in terms of the ocean's ability to remove carbon from the atmosphere, being responsible for ~ 40% of the global ocean uptake of anthropogenic CO_2 (Khatiwala et al., 2009). Improved data coverage in the Southern Ocean represents thus a major opportunity to advance our understanding of the global ocean carbon sink (Lenton et al., 2006, 2013; Takahashi et al., 2009; Monteiro et al., 2015; Gregor et al., 2019; Gray et al., 2018; Mongwe et al., 2018; Bushinsky et al., 2019; Sutton et al., 2021; Long et al., 2021; Mackay et al., 2022; Wu et al., 2022; Landschützer et al., 2023). A combination of SOCAT and Saildrone USV observations would include high accuracy data from both the long record and global coverage of ship tracks, and the expanded finer resolution of spatial and seasonal coverage of the poorly sampled Southern Ocean. Importantly, Saildrone USVs are also able to cover the spatial extent and seasonal cycle of the meridional gradients, which has been shown to be critical in order to reduce errors in reconstructing surface ocean pCO_2 (Djeutchouang et al., 2022). A combined approach, with autonomous samples such as those obtained from Saildrone USVs, in addition to high-quality observations collected from ships, represents thus a promising solution to improve surface ocean pCO_2 ML reconstructions.

Here, we assess to what extent surface ocean pCO_2 reconstructions can improve by implementing the pCO_2-Residual machine learning (ML) reconstruction (Bennington et al., 2022a) with the combined inputs of SOCAT and Saildrone USV coverage. However, instead of using actual observations, we sample the target (i.e., surface ocean pCO_2) and driver variables (i.e., SST, SSS, MLD, Chl-a and xCO_2) from our Large Ensemble Testbed (LET) of Earth System Models (ESMs) (e.g., Stamell et al., 2020; Gloege et al., 2021; Bennington et al., 2022a). There are two major benefits of using a testbed compared to actual observations. First, in an ESM, surface ocean

pCO_2 is known at all times and locations. Therefore, the pCO_2 reconstructed by the ML algorithm can be robustly evaluated in space and time against a known 'truth' (i.e., 'model truth'). The reconstruction evaluation is thus not limited to the availability of sparse real-world ocean observations. Secondly, a testbed can be used to plan and evaluate the impact of different sampling strategies on the reconstructed pCO_2. It is important to stress that, by using a model testbed, we do not predict real-world surface ocean pCO_2 and air-sea CO_2 fluxes. The goal here is to assess the accuracy with which an ML algorithm can reconstruct the 'model truth' given inputs of samples consistent with real-world data coverage from the SOCAT database and Saildrone USVs.

By utilizing the observational coverage of SOCAT and Saildrone USV transects, we assess to what extent the pCO_2-Residual method accurately reconstructs model surface ocean pCO_2 in space and time. Additionally, we explore the timing, magnitude, duration and spatial extent of Southern Ocean USV sample additions that most significantly improve the pCO_2 predictions.

2. Methods

2.1 The Large Ensemble Testbed (LET)

In this study, the Large Ensemble Testbed (LET) includes 25 members from three independent initial-condition ensemble models (i.e., CanESM2, CESM-LENS and GFDL-ESM2M; Kay et al., 2015; Rodgers et al., 2015; Fyfe et al., 2017), giving a total of 75 members within the testbed. We do not use the MPI-GE model that was included in the past LET studies because its Southern Ocean pCO_2 seasonality and decadal variability appears to be anomalously large (Gloege et al., 2021; Fay and McKinley, 2021; Bennington et al., 2022a). Each individual Earth System Model (ESM) is an imperfect representation of the actual Earth system, so the multiple Large Ensembles are used to span different model structures and their representation of internal variability. Each ensemble member undergoes the same external forcing (i.e., historical atmospheric CO_2 before 2005 and Representative Concentration Pathway 8.5 through 2016, plus solar and volcanic forcing), but the spread across the ensemble members gives a unique trajectory of the ocean-atmosphere state over time, i.e., a different state of internal variability as well as the difference across models.

The LET used in this study includes monthly 1°x1° model output from 1982-2016 (Gloege et al., 2021). For each individual ensemble member of the LET, surface ocean pCO_2 and co-located driver variables (i.e., SST, SSS, Chl-a, MLD, xCO_2) were sampled monthly at a 1°x1° resolution, at times and locations equivalent to SOCAT and Saildrone USV observations (**Fig. 1**; Step 1). While the SOCAT observations were sampled from the testbed matching the actual years of sampling, the USV observations were sampled from the testbed starting in year 2007 (for ten-year sampling) or 2012 (for five-year sampling) (see **Sect. 2.4**). As our focus is on reconstruction for the open ocean, testbed output for coastal areas, the Arctic Ocean (>79°N) and marginal seas (Hudson Bay, Caspian Sea, Black Sea, Mediterranean Sea, Baltic Sea, Java Sea, Red Sea and Sea of Okhotsk) were removed prior to algorithm processing.

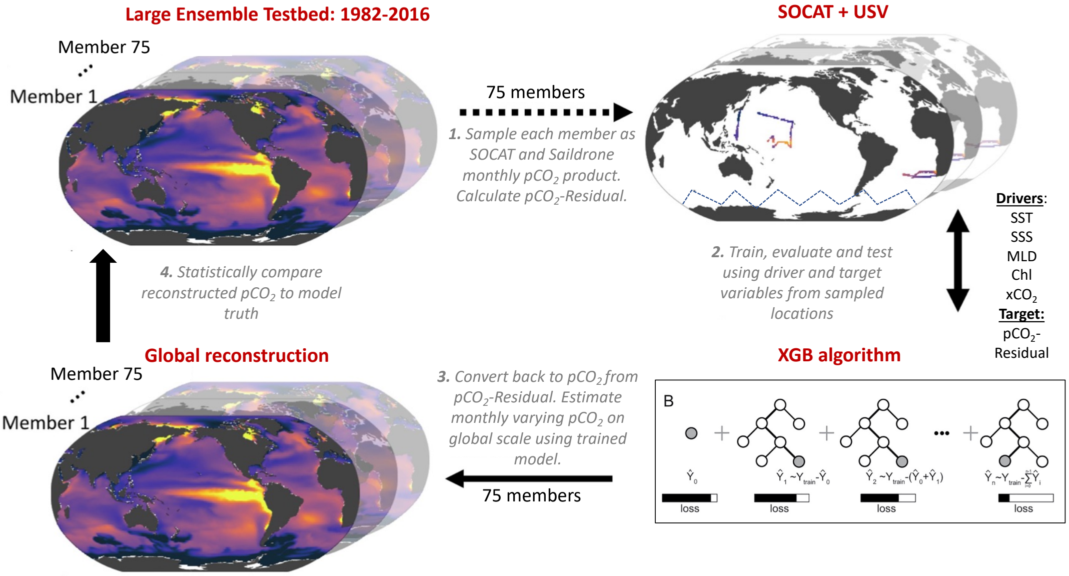
Large Ensemble Testbed: 1982-2016
Member 75
Member 1
75 members
1. Sample each member as SOCAT and Saildrone monthly pCO_2 product. Calculate pCO_2-Residual.
SOCAT + USV
Drivers:
SST
SSS
MLD
Chl
xCO_2
Target:
pCO_2-Residual
2. Train, evaluate and test using driver and target variables from sampled locations
4. Statistically compare reconstructed pCO_2 to model truth
Global reconstruction
Member 75
Member 1
3. Convert back to pCO_2 from pCO_2-Residual. Estimate monthly varying pCO_2 on global scale using trained model.
75 members
XGB algorithm
B
$\hat{Y}_0$
$\hat{Y}_1 \sim Y_{train} - \hat{Y}_0$
$\hat{Y}_2 \sim Y_{train} - (\hat{Y}_0 + \hat{Y}_1)$
$\hat{Y}_n \sim Y_{train} - \sum_{i=0}^{n-1} \hat{Y}_i$
loss
loss
loss
loss

Figure 1: Schematic of the Large Ensemble Testbed (LET; modified from Gloege et al., 2021). **1:** Surface ocean pCO_2 from each of the 75 model members is sampled in space and time mimicking real-world SOCAT and Saildrone USV observations (see **Fig. 2**; **Table 1**; **Section 2.5**). Prior to algorithm processing, pCO_2-Residual is calculated, i.e., the direct effect of temperature has been removed from the pCO_2 value (**Section 2.2**). **2:** The pCO_2-Residual (target variable) and co-located driver variables (i.e., SST, SSS, MLD, Chl, xCO_2) sampled from the testbed are processed by the XGBoost (XGB) algorithm (**Section 2.3**). **3:** Based on the full-coverage of driver variables, pCO_2-Residual is reconstructed globally. This process is repeated 75 times, individually for every single testbed model member. The temperature component (pCO_2-T) is then added back to the pCO_2-Residual for each value. **4:** Since we are using model testbed and not real-world observations, the globally reconstructed pCO_2 can be evaluated against the 'model truth' at all 1°x1° grid cells, not just where observations are available. SST = sea surface temperature. SSS = sea surface salinity. MLD = mixed layer depth. Chl = chlorophyll. xCO_2 = atmospheric concentration of CO_2.

https://doi.org/10.5194/bg-2023-160
Preprint. Discussion started: 10 October 2023

2.2 The pCO_2-Residual approach

We used the pCO_2-Residual approach following Bennington et al. (2022a), which removes the well-studied direct effect of temperature on pCO_2 from the LET model output prior to algorithm processing. Temperature has both direct and indirect effects on surface ocean pCO_2. The direct effect of temperature, due to solubility and chemical equilibrium, is that an increase in temperature directly causes an increase in pCO_2 (Takahashi et al., 1993). Indirectly, temperature changes are associated with biological production and wintertime vertical mixing; and these processes tend to result in opposing pCO_2 changes. To build reconstruction algorithms through the data-driven training that occurs in ML, the statistics in all other algorithms developed to date must identify a function that disentangles these competing effects of SST on pCO_2. Here, the algorithm is assisted by removing this known temperature effect, and it must therefore only learn the pCO_2 impacts from biogeochemical drivers. The pCO_2-Residual method leads to physically understandable connections between the input data and output (Bennington et al., 2022a), which mitigates to some degree 'black box' concerns typically associated with ML algorithms (Toms et al., 2020). Further, this method has been shown to perform better against independent observations than other common observation-based products (Bennington et al., 2022a). A brief description is provided here, but for further details see Bennington et al. (2022a).

The temperature-driven component of pCO_2 (pCO_2-T) is calculated using this equation:

$$pCO_2\text{-T} = pCO_2^{mean} * \exp[0.0423 * (SST - SST^{mean})]$$

where pCO_2^{mean} and SST^{mean} is the long-term mean of surface ocean pCO_2 and temperature, respectively, using all 1°x1° grid cells from the testbed. Once pCO_2-T is determined, pCO_2-Residual is calculated as the difference between pCO_2 and the calculated pCO_2-T:

$$pCO_2\text{-Residual} = pCO_2 - pCO_2\text{-T}$$

Prior to algorithm processing, pCO_2-Residual values > 250 µatm and < -250 µatm from the testbed were filtered out to target values that are not representative of the real ocean. These pCO_2-Residual values generally correspond to high pCO_2, above the maximum value in SOCAT (816 µatm; Stamell et al., 2020). The excluded data points (less than 0.2 % per member) mostly occurred in output from the CanESM2 model, and were restricted geographically, predominantly along the western coastline of South America.

The eXtreme Gradient Boosting method (XGB; Chen and Guestrin, 2016) is used to develop an algorithm that allows driver variables (i.e., SST, SSS, Chl-a, MLD, xCO_2) to predict the pCO_2-Residual (**Fig. 1**; Step 2). The pCO_2-Residual and associated feature variables is split into validation, training and testing sets. The test and validation set each account for 20 % of the data, leaving 60 % for training. The validation set is used to optimize the algorithm hyperparameters, which define the architecture of decision trees used in the model. The training set is used to build the decision trees in XGB, while the test set is used to evaluate the performance of the final algorithm. The XGB algorithm for this study used 4,000 decision trees with a maximum depth of 6 levels. For the final reconstruction of surface ocean pCO_2 across all space and time points, the previously calculated pCO_2-T values are added back to the reconstructed pCO_2-Residual (**Fig. 1**; Step 3).

The full XGB process, including 1) training/evaluating/testing and 2) reconstructing globally at a monthly resolution, was repeated individually for each LET member. This process provided therefore a total of 75 unique reconstruction vs. 'model truth' pairs, which can be statistically compared (**Fig. 1**; Step 4).

2.3 Statistical Analysis in the Testbed

The statistical comparisons between the test set and the reconstructions are equivalent to what would be derived using real-world data ('seen' values). Since we are using a testbed, we can also include comparisons on additional independent data, referred to as 'unseen' values, which represent the 1°x1° grid cells of the ensemble members that do not correspond to SOCAT or Saildrone USV observations. A suite of statistical metrics can be used to compare the reconstruction to the 'model truth' in order to assess how well the algorithm can extrapolate from sparse data to full-field coverage (**Fig. 1**; Step 4). In this study, we focus on bias and root-mean-squared error (RMSE). Bias is calculated as 'mean prediction – mean observation' (i.e., pCO_2 predicted by XGB subtracted by the pCO_2 'model truth'), and is a measure of over- or underestimation in the reconstructions. RMSE measures the magnitude of the predicted error and is calculated as the square root of the mean of the squared errors.

https://doi.org/10.5194/bg-2023-160
Preprint. Discussion started: 10 October 2023

2.4 Overview of sampling patterns and model runs

First, we sampled target and driver variables from the LET based on sampling distributions equivalent to that of the SOCAT database ('SOCAT baseline'). Then, we combined the 'SOCAT baseline' with testbed output representing additional Saildrone USV coverage in the Southern Ocean. The additional Southern Ocean coverage was based on 1) the Sutton et al. (2021) sampling campaign from 2019 ('one-latitude' track) and 2) potential future meridional USV observations ('zigzag' track) (**Fig. 2**). We performed a total of 10 experimental runs (**Table 1**). These represent different sampling approaches, including: 1) repeating USV sampling over a five- or ten-year period, 2) varying the number of USVs and thus the total number of observations, and 3) restricting all observations to southern hemisphere winter months. By comparing the different runs, we can assess whether or not certain targeted sampling strategies in the Southern Ocean can improve surface ocean pCO_2 ML reconstructions. As discussed above, the LET runs to 2016 only (Gloege et al., 2021). Saildrone USV observations were therefore sampled from the testbed starting in year 2006 or 2007 (for the ten-year sampling) or 2012 (for the five-year sampling) until 2016, i.e., the final year of the testbed.

2.4.1 'One-latitude' runs

Six out of the ten experimental runs include the 'one-latitude' track (**Table 1**). The 2019 Saildrone USV journey (Sutton et al., 2021) covered an 8-month period, from January to August. Since the USV was recovered in early August, it did not cover the entire southern hemisphere winter (**Fig. S1**). We repeated this 'one-latitude' eight-month sampling pattern for five years ('5Y_J-A'; 2,075 observations) and ten years ('10Y_J-A'; 4,150 observations). In order to evaluate year-round ('YR') coverage, the eight-month sampling period (January-August) was shifted by one month each year for ten years ('10Y_YR'; 4,150 observations). Furthermore, in order to evaluate the impact of increased sampling, the 2019 Saildrone USV track was repeated 12 times with incremental offsets of 1° from the original track, covering an additional 6° north and south (**Fig. S2**). This 'high-sampling'-run ('x13_10Y_J-A'; 44,250 observations) represents a total of 13 USVs. We also performed an additional 13 USV run, but including observations from southern hemisphere winter ('W') months only ('x13_10Y_W'; 25,395 observations). Finally, considering the cost of deploying 13 USVs, a downscaled 'multiple-USV-winter-only'-run was tested, including five USVs sampling over a period of five years ('x5_5Y_W'; 5,022 observations). This run covers an additional 2° north and south from the original USV track.

2.4.2 'Zigzag' runs

Four of the ten experimental runs represent potential meridional sampling in the Southern Ocean ('zigzag' tracks; **Table 1**) as suggested by Djeutchouang et al. (2022). Due to limited solar radiation that powers the Saildrone USVs, we let the sampling occur at a maximum latitude of 55° S. This alternative sampling pattern represents USVs sailing west to east in a north/south 'zigzag' pattern covering 40° S and 55° S for every 30° of longitude (**Fig. 2**). We created two scenarios. For the first scenario, every 30° of longitude from 40° S and 55° S is visited every three months within a single year as suggested by Lenton et al. (2006). Considering the average Saildrone USV speed, this scenario represents four platforms equally spaced around the Southern Ocean. This sampling pattern was repeated for 10 years, with year-round coverage ('Zx4_10Y_YR'; 7,600 observations), and for southern hemisphere winter months only ('Zx4_10Y_W'; 2,500 observations). The second scenario represents a 'high-sampling' strategy, where every 30° of longitude from 40° S and 55° S is visited approximately monthly. This can be achieved by deploying 10 platforms equally spaced around the Southern Ocean. This sampling pattern is repeated for five years, sampling year-round ('Z_x10_5Y_YR'; 11,400 observations) and during southern hemisphere winter months only ('Z_x10_5Y_W'; 3,800 observations).

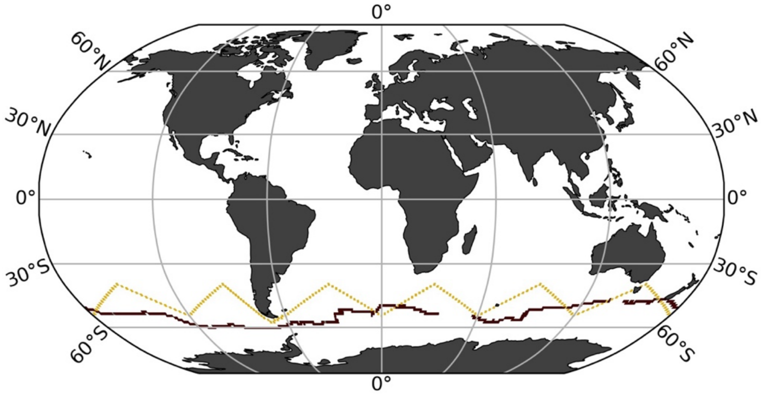

Figure 2: Saildrone Uncrewed Surface Vehicle (USV) tracks representing the first circumnavigation around Antarctica from 2019 in maroon ('one-latitude' track; Sutton et al., 2021) and an alternative virtual route with meridional coverage ('zigzag' track).

Run name	5Y_J-A	10Y_J-A	10Y_YR	x13_10Y_J-A	x13_10Y_W	x5_5Y_W	Z_x4_10Y_YR	Z_x4_10Y_W	Z_x10_5Y_YR	Z_x10_5Y_W
Saildrone track	One-lat	One-lat	One-lat	One-lat	One-lat	One-lat	Zigzag	Zigzag	Zigzag	Zigzag
Years of sampling	5	10	10	10	10	5	10	10	5	5
# of Saildrones	1	1	1	13	13	5	4	4	10	10
Duration of sampling	Jan-Aug	Jan-Aug	Year-round	Jan-Aug	SO winter	SO winter	Year-round	SO winter	Year-round	SO winter
Total observations	**2,075**	**4,150**	**4,150**	**44,250**	**25,395**	**5,022**	**7,600**	**2,500**	**11,400**	**3,800**
Global coverage increase (%)	0.01	0.02	0.02	0.2	0.1	0.02	0.03	0.01	0.04	0.01

Table 1. Overview of the different Saildrone USV sampling patterns tested in this study using the XGBoost Machine Learning algorithm (Gloege et al., 2021; Bennington et al., 2022a) to estimate surface ocean pCO_2. The 'one-latitude' ('one-lat') track incorporate the Saildrone USV route from Sutton et al. (2021), while the 'zigzag' track represents potential future meridional sampling (see **Fig. 2**). The total number of USV observations (in bold) represent 1°x1° monthly Saildrone USV observations. J-A= January-August. YR = year-round. W = southern hemisphere winter. x4, x5, x10 and x13 = four, five, ten and 13 USVs. SO winter = Southern Ocean winter months, i.e., June, July, August and also including September. Note that all runs also included SOCAT coverage.

2.5 Air-sea CO_2 flux

To assess the global ocean carbon sink associated with our pCO_2 reconstructions, air-sea CO_2 exchange was calculated. Here, we computed air-sea CO_2 fluxes using the bulk formulation with python package Seaflux.1.3.1 (https://github.com/lukegre/SeaFlux; Gregor et al. 2021; Fay et al., 2021). We calculated global and Southern Ocean flux in the same manner for 1) the testbed 'model truth', 2) the SOCAT baseline and 3) the 10 experimental USV runs.

The net sea–air CO_2 flux was estimated using:

$$\mathrm{Flux}=k_W\cdot \mathrm{sol}\cdot(pCO_2^{ocn}-pCO_2^{atm})\cdot(1-\mathrm{ice})$$

where 'k_W' is the gas transfer velocity, 'sol' is the solubility of CO_2 in seawater (in units of mol m^{-3} μatm^{-1}), 'pCO_2^{ocn}' is the partial pressure of surface ocean carbon (in μatm), either from the 'model truth' or from the reconstructions, and pCO_2^{atm} (in μatm) is the partial pressure of atmospheric CO_2 in the marine boundary layer. For GFDL, we used direct model output of pCO_2^{atm}, while for CESM and CanESM2, pCO_2^{atm} was calculated individually, as the product of surface xCO_2 and sea level pressure (pCO_2^{atm} from CESM was corrected for the contribution of water vapor pressure). Finally, to account for the seasonal ice cover in high latitudes, the fluxes were weighted by 1 minus the ice fraction ('ice'), i.e., the open ocean fraction. Inputs to the calculation include EN4.2.2 salinity (Good et al., 2013), SST and ice fraction from NOAA Optimum Interpolation Sea Surface Temperature V2 (OISSTv2) (Reynolds et al., 2002), and surface winds and associated wind scaling factor from the European Centre for Medium-Range Weather Forecasts (ECMWF ERA5 sea level pressure (Hersbach et al., 2020). Results presented show the global and Southern Ocean (< 35° S) fluxes in units of Pg C yr^{-1}.

Note that, reconstructions of pCO_2 for the SOCAT baseline and the experimental USV runs are limited in their spatial extent to the open ocean (see **Sect. 2.1**; excluding coastal areas, the Arctic Ocean and marginal seas). The same mask was thus also applied when calculating the flux of the 'model truth', prior to comparison with the reconstructions.

3. Results

3.1 Performance metrics for the 'SOCAT baseline' reconstruction

The mean bias for the entire testbed period (i.e., 1982-2016) is 0.63 µatm globally (**Fig. 3a**) and 1.4 µatm for the Southern Ocean (< 35° S; **Table S1**). Bias is much closer to zero for mid- (between 35° S and 35° N; 0.23 µatm) and northern latitudes (> 35° N; 0.11 µatm) (**Fig. 3a**). There is a significant difference in bias considering southern hemisphere winter months (June, July, August) versus summer months (December, January, February), with a global mean bias (for 1982-2016) of 1.3 µatm compared to 0.07 µatm, respectively (**Table S1**), due to the sparseness of SOCAT observations from the southern hemisphere during the harsh winter season (**Fig. S3a**). The mean RMSE for the entire testbed period (i.e., 1982-2016) is 7.9 µatm globally (**Fig. 3b**) and 8.5 µatm for the Southern Ocean (**Table S1**). RMSE is highest in the Eastern Tropical and Southeastern Pacific Ocean and in the Southern Ocean, where the algorithm generally overestimates pCO_2 (i.e., positive bias; **Fig. 3a**). This is consistent with the areas significantly undersampled by SOCAT (**Fig. S3b**). Except for these areas, RMSE and bias is generally low (close to zero) in the open ocean, but show higher values along coastlines (**Fig. 3b**).

https://doi.org/10.5194/bg-2023-160
Preprint. Discussion started: 10 October 2023

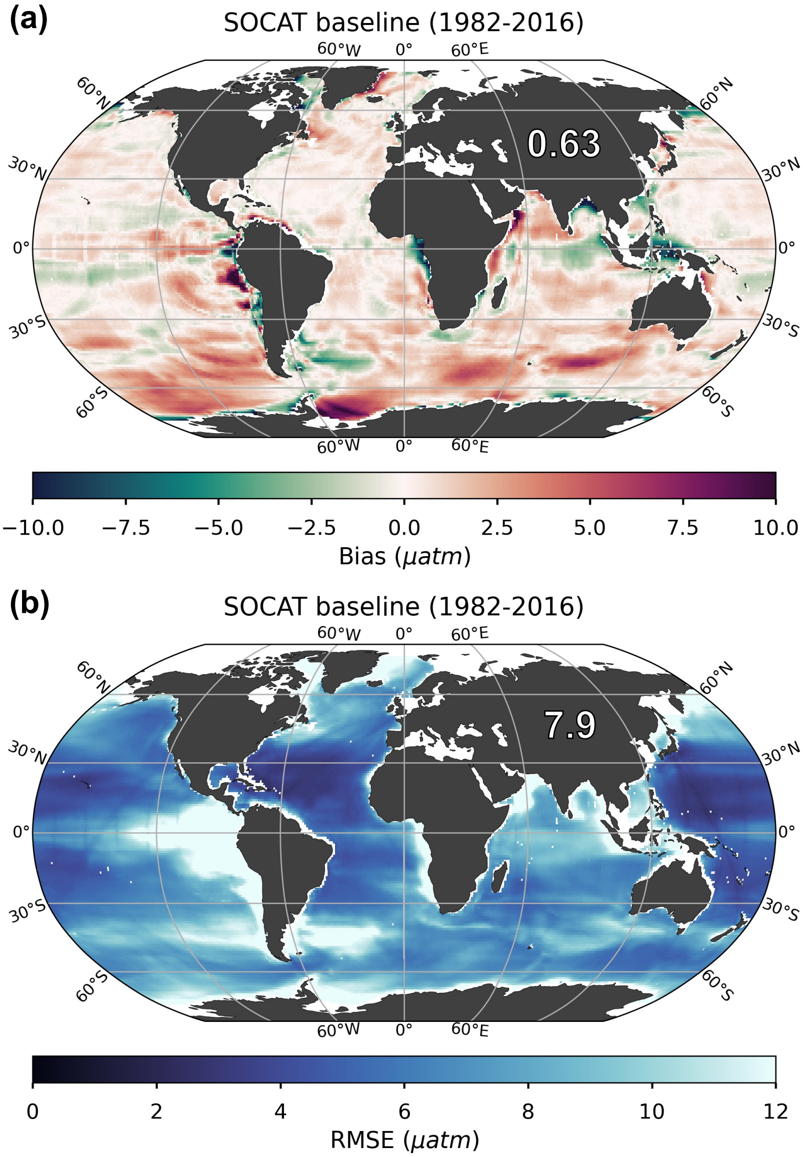

Figure 3: Bias (**a**) and root-mean-squared error (RMSE) (**b**) when comparing the baseline machine learning reconstruction with the testbed 'model truth', averaged over the 75 ensemble members for the period of 1982 through 2016. The testbed was sampled based on SOCAT observations only (i.e., no USV). The global mean bias and RMSE is 0.63 µatm and 7.9 µatm, respectively. Red and green areas in **a** indicate regions where the reconstruction is biased high (i.e., overestimates pCO_2) and low (i.e., underestimates pCO_2), respectively. Generally, RMSE is highest in the East and South Pacific Ocean and in the Southern Ocean, where the algorithm also generally overestimates pCO_2 (positive bias; **a**). Note that only the open ocean was considered in the reconstruction, so several areas were masked out prior to algorithm processing, such as the Arctic Ocean, coastal areas and marginal seas (no data; white areas in figures).

3.2 Reconstruction improvements with Saildrone USV additions

Our presentation of global maps is limited to runs 'x5_5Y_W' (5,022 observations) and 'Z_x4_10Y_YR' (7,600 observations). These runs were selected as they represent observational schemes that are realistic in the near-term future considering logistics and cost level, both non-meridional and meridional sampling, and different approaches to observing duration and seasonal coverage. For the remaining runs, equivalent maps can be found in the **Supplement**.

3.2.1 Bias

All Saildrone USV runs show a reduction in bias compared to the global mean 1982-2016 SOCAT baseline (**Figs. 4a**, **S4**). The improvement in bias is mainly due to lower reconstructed pCO_2 values at southern latitudes, where the baseline reconstruction generally overestimates pCO_2 (**Fig. 3a**). The global mean bias for 'zigzag' run 'Z_x4_10Y_YR' is 0.51 µatm, a higher improvement (19 %) over the SOCAT baseline compared to the 'one-latitude' run 'x5_5Y_W' (11 % improvement; mean bias = 0.57 µatm;) (**Fig.4a**; **Table S1**). Generally, the 'zigzag' runs show higher improvements from the SOCAT baseline (19-31 % improvement; mean bias = 0.44-0.51 µatm) compared to the 'one-latitude' runs (7-19 % improvement; mean bias = 0.52-0.59 µatm) (**Fig S4**; **Table S1**). However, the 'one-latitude'-run 'x13_10Y_W' that samples southern hemisphere winter months only, stands out with the lowest global mean bias of 0.39 µatm, representing a 39 % improvement from the SOCAT baseline (**Table S1**; **Fig. S4**). This run, however, has three or five times more observations (25,395) than 'Z_x4_10Y_YR' and 'x5_5Y_W', respectively.

Compared to the entire testbed period, even larger improvements in global mean bias are shown for the period of Saildrone USV additions (2006-2016 and 2012-2016; **Figs. 4a** vs. **4b**, **Figs. S4** vs. **S5**). Compared to the SOCAT baseline, run 'x13_10Y_W' results in a bias improvement of 95 %, while the remaining 'one-latitude' runs and the 'zigzag' runs show improvements up to 63 % and 85 %, respectively (**Fig. S5**).

Perhaps surprisingly, there is not a strong connection between the global or Southern Ocean mean bias and the number of added USV observations (**Fig. 5**). The 'one-latitude' 'high-sampling' run 'x13_10Y_J-A' (44,250 observations) show similar bias or is outperformed by all 'zigzag' runs as well as the 'one-latitude'-runs that restrict sampling to southern hemisphere winter months (i.e., 'x5_5Y_W' and 'x13_10Y_W').

Considering the change in bias from year-to-year, the SOCAT baseline shows positive bias at all latitudes in the beginning of the testbed period, before improvement occurs around year 1990 (**Fig. 6a**). This is consistent with increasing SOCAT sampling with time for the time period considered here (i.e., up to 2016; **Fig. S3c**). As SOCAT observations are biased towards the northern hemisphere (**Fig. S3a, b**), bias in the Southern Ocean (< 35° S) increases significantly starting in 2000s and remains high until the end of the testbed period (**Fig. 6a**). By adding USV sampling, bias in the Southern Ocean improves over the SOCAT baseline around year 2000 (**Fig. 6b-d**; **Fig. S6**), up to 6-12 years prior to the introduction of additional samples in either 2006 or 2012. Run 'Z_x10_5Y_W', which has the lowest bias out of the 'zigzag' runs (**Fig. 5**), shows improvement even further back in time, until the beginning of the testbed period (**Fig. S6**). While the annual mean bias of the 'zigzag' runs vary in a similar manner, there is a large spread between the 'one-latitude' runs (**Fig. 6d**).

https://doi.org/10.5194/bg-2023-160
Preprint. Discussion started: 10 October 2023

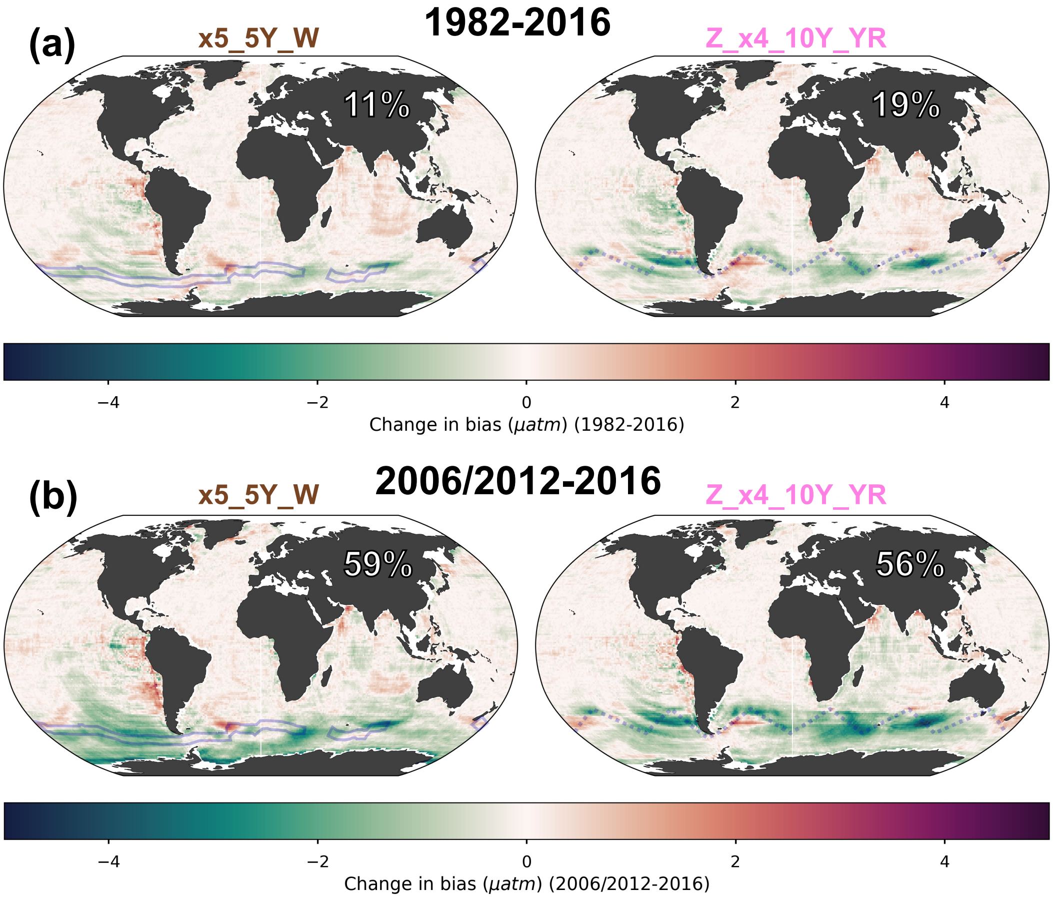

Figure 4: Change in bias when comparing run 'x5_5Y_W' and 'Z_x4_10Y_YR' to the SOCAT baseline reconstruction, averaged over the duration of the testbed period (**a**; 1982-2016) and the period of USV additions (**b**; 2006-2012 or 2012-2016). Negative change in bias is found across the southern latitudes, indicating an improvement compared to the SOCAT baseline that overestimates pCO_2 (**Figure 3a**). The percent global improvement is shown on each panel. Note that improvement is greater in the period of Saildrone USV additions compared to the entire testbed period.

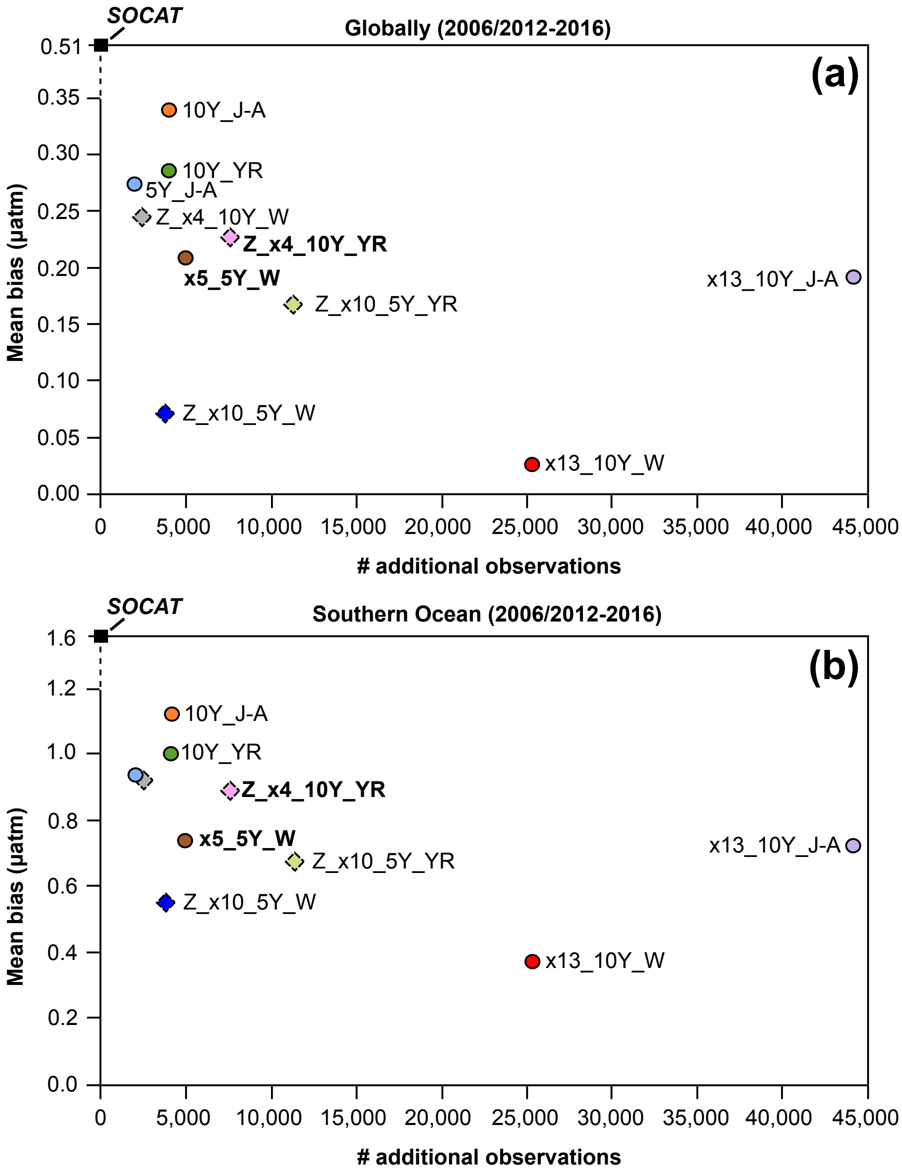

Figure 5: Mean bias globally (**a**) and for the Southern Ocean (**b**) for the duration of Saildrone USV sampling (2006-2016 or 2012-2016) for all runs presented in **Table 1**. Circles represent runs using the 'one-latitude' track (Sutton et al., 2021), while diamonds represent 'zigzag' runs. Runs highlighted in bold correspond to the two selected runs mapped in **Figure 4, 6, 7** and **9**. Global (0.51 µatm) and Southern Ocean (1.6 µatm) bias values shown for the SOCAT baseline (black squares) represent a mean of values for 2006-2016 (global = 0.52 µatm, S. Ocean = 1.63 µatm) and 2012-2016 (global = 0.51 µatm, S. Ocean = 1.56 µatm). The SOCAT baseline run included 261,733 monthly 1°x1° observations. Overall, there is not a strong correlation between bias and the number of observations, or duration of sampling.

https://doi.org/10.5194/bg-2023-160
Preprint. Discussion started: 10 October 2023

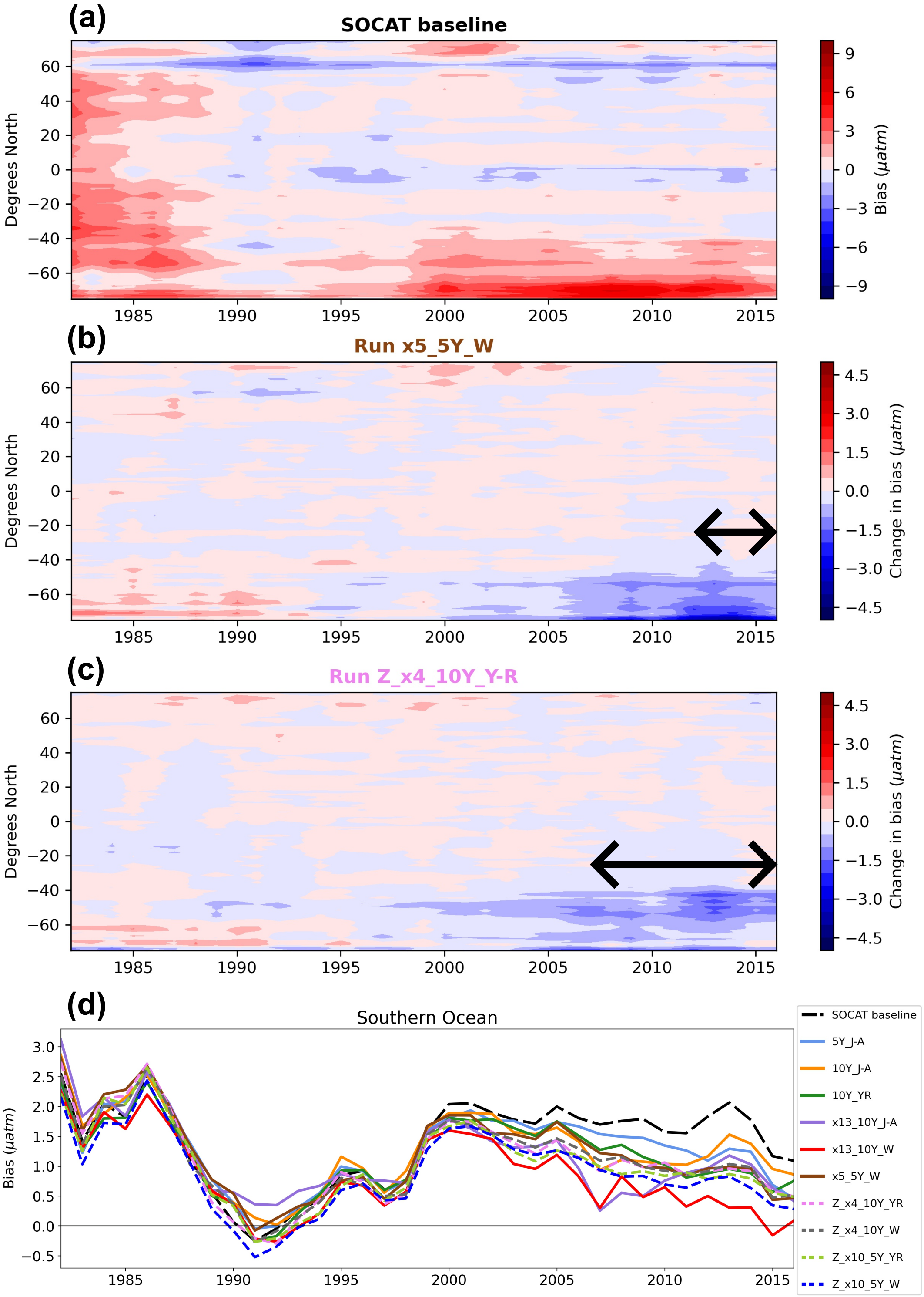

369

Figure 6: Zonal mean, annual mean Hovmöller of bias in SOCAT baseline with the testbed 'model truth', average of 75 ensemble members (**a**). There is a positive bias at all latitudes from 1982-1995; bias drops to around zero in the late 1980s; and then, particularly in the Southern Ocean, increases at 2000 and remains high through 2016. Change in bias of run 'x5_5Y_W' (**b**) and 'Z_x4_10Y_YR' (**c**)compared to the SOCAT baseline reconstruction shown in (**a**). Negative changes in the Southern Ocean represents an improvement. The improvement in bias expands back in time well beyond the duration of USV additions for both runs (shown by arrows on each panel). Annual mean bias for the Southern Ocean (> 35° S) for all runs(**d**). There is a large spread in the impact on bias with 'one-latitude' USV sampling (solid lines), while the 'zigzag' runs (dashed lines) more consistently reduce bias.

3.2.2 Root-mean squared error (RMSE)

Similar to bias, improvements in RMSE are most significant during the period of USV additions and within the Southern Ocean (**Fig. 7a** vs. **7b**). For the duration of USV additions, the 'one-latitude' runs show improvements in global mean RMSE of 1-4 % (0.3-2 % for 1982-2016), while the 'zigzag' runs show higher improvements between 3-8 % (2-3 % for 1982-2016) (**Figs. 7**, **S7, S8**). RMSE is further reduced in southern hemisphere winter in the Southern Ocean by up to 26 % (mean RMSE of 6.9 µatm; **Table S1**). There is minimal change in RMSE (or bias) during southern hemisphere summer months (DJF; **Fig. S9)**. The two 'zigzag' runs sampling year-round ('Z_x4_10Y_YR' and ''Z_x10_5Y_YR) have the lowest RMSE values both globally and in the Southern Ocean (**Fig. 8**).

The 'zigzag' runs, as well as the 'high-sampling' 'one-latitude'-runs (i.e., 'x13_10Y_J-A' and 'x13_10Y_W'), show improvements compared to the SOCAT baseline from the initiation of sampling (**Figs. 9**, **S10**). The year-round 'zigzag' runs, however, show improvement in the Southern Ocean from the beginning of the testbed period (**Figs. 9c**, **d**, **S10**). RMSE improvements back in time are more significant for all runs in the southern hemisphere winter months (**Fig. S11**).

https://doi.org/10.5194/bg-2023-160
Preprint. Discussion started: 10 October 2023

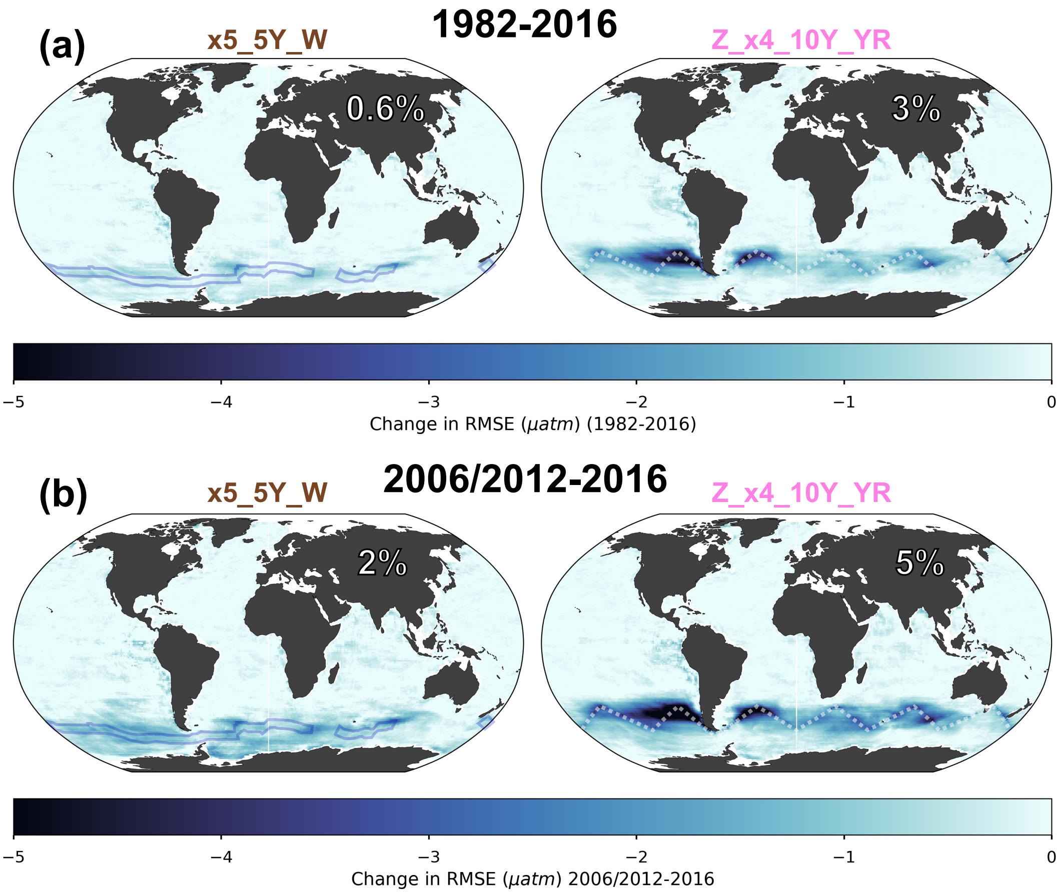

Figure 7: Change in RMSE when comparing run 'x5_5Y_W' and 'Z_x4_10Y_YR' to the SOCAT baseline reconstruction, averaged over the duration of the testbed period (**a**; 1982-2016) and the period of Saildrone USV additions (**b**; 2006-2012 or 2012-2016). Improvement in RMSE occurs mainly in southern latitudes (<35°S), where the baseline reconstruction shows high RMSEs (**Fig. 3b**). The percent global improvement is shown on each panel. Note the greater improvement for the period of USV additions compared to the entire testbed period.

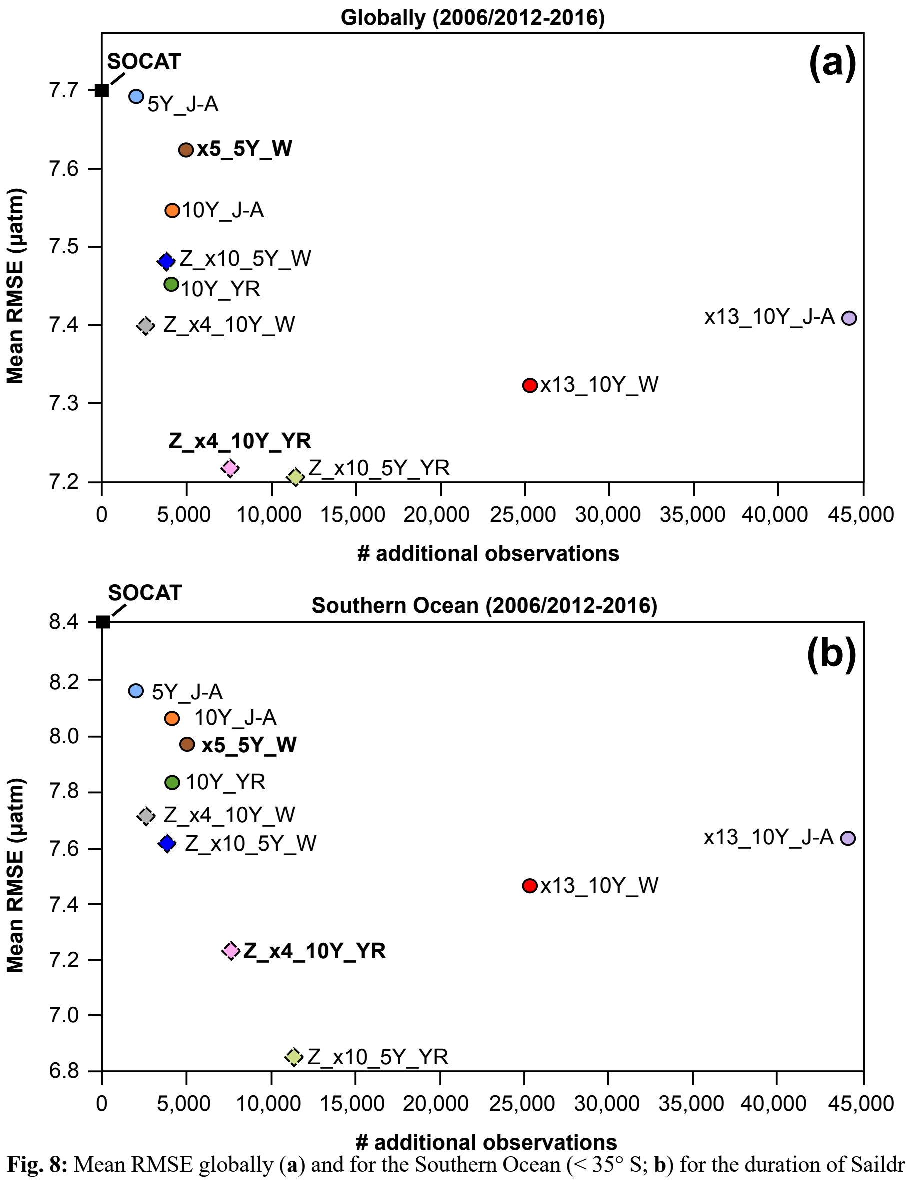

Fig. 8: Mean RMSE globally (**a**) and for the Southern Ocean (< 35° S; **b**) for the duration of Saildrone USV sampling (2006-2016 or 2012-2016) for all runs presented in **Table 1**. 'One-latitude' runs (circles), 'zigzag' runs (diamonds). Runs highlighted in bold correspond to the two selected runs mapped in **Figure 4, 6, 7** and **9**. Global (7.7 µatm) and Southern Ocean (8.4 µatm) bias values shown for the SOCAT baseline (black squares) represent a mean of values for 2006-2016 (global = 7.6 µatm, S. Ocean = 8.3 µatm) and 2012-2016 (global = 7.8 µatm, S. Ocean = 8.5 µatm). The SOCAT baseline run included 261,733 monthly 1°x1° observations. Overall, there is not a strong correlation between increasing number of observations or duration of sampling and decreasing RMSE.

https://doi.org/10.5194/bg-2023-160
Preprint. Discussion started: 10 October 2023

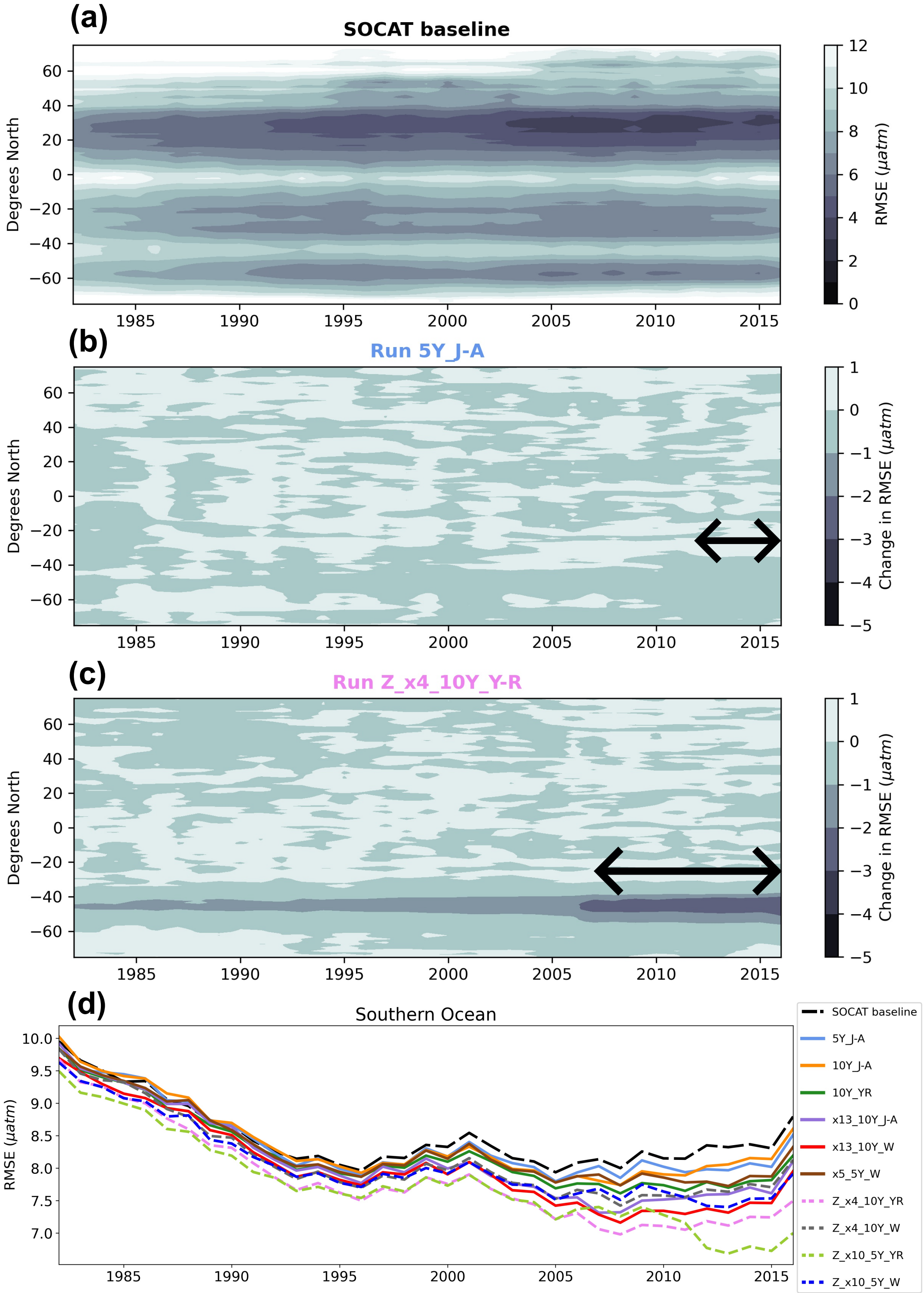

Figure 9: Zonal mean, annual mean Hovmöller of RMSE in SOCAT baseline with the testbed 'model truth', average of 75 ensemble members (**a**). Dark and light areas represent regions where RMSE is low and high, respectively. RMSE is highest at latitudes > 60° S, > 60° N and around 40° S and the equator. RMSE is higher at all latitudes in the beginning of the testbed period, before some improvement occurs in the 1990s. Change in RMSE of run 'x5_5Y_W' (**b**) and 'Z_x4_10Y_YR'(**c**) compared to the SOCAT baseline reconstruction shown in (**a**). Dark areas represent regions where the change in RMSE is negative, i.e., where the Saildrone USV sampling additions improve the pCO_2 reconstruction. Run 'Z_x4_10Y_YR' shows improvements in RMSE within the Southern Ocean, which expand well beyond the duration of Saildrone USV additions (shown by arrow on panel). Annual mean RMSE for the Southern Ocean (> 35° S) for all runs (**d**).

3.3 Impact on the air-sea CO_2 flux with Saildrone USV additions

Air-sea flux was calculated in the same manner for both the ML reconstructions and the 'model truth', which allows for direct comparison of the differences in fluxes (see **Sect. 2.5**). These flux estimates are made to inform understanding of the errors that may exist in CO_2 flux estimates derived from pCO_2 reconstructions, and how new sampling could address these errors. These fluxes are not estimates of real-world fluxes.

Compared to the 'model truth', the SOCAT baseline reconstruction underestimates the global and Southern Ocean sink by 0.11-0.13 Pg C yr^{-1} over 1982-2016 (**Fig. 10**; **Table S2**). Regardless of sampling pattern, adding Saildrone USV observations increases both the global and Southern Ocean mean sink compared to the SOCAT baseline (**Figs. 10**, **S12**). The 'one-latitude' runs show an increase of 0.01-0.03 Pg C yr^{-1} (2-6 % strengthening) of the Southern Ocean sink (1982-2016), while the 'zigzag' runs lead to an even stronger sink 0.04-0.06 Pg C yr^{-1} (7-11 % strengthening) (**Table S3**). When averaging over the years of Saildrone USV sampling addition (i.e., 2006-2012 and 2012-2016), the Southern Ocean sink increases up to 0.09 Pg C yr^{-1} (14 % strengthening) for the 'one-latitude' runs and up to 0.1 Pg C yr^{-1} (15 % strengthening) for the 'zigzag' runs (**Table S3**). These same features are found for the global ocean (**Fig. S12**; **Table S3**).

All of the 'zigzag' runs quite closely match both the global and Southern Ocean 'model truth' air-sea CO_2 flux for the duration of sample additions (**Figs. 10**, **S12**). Except for the first couple of years of sample addition for the 'high-sampling'-run 'x13_10Y_J-A', none of the 'one-latitude' runs are able to match the 'model truth' air-sea CO_2 flux, as they all underestimate the flux (**Figs. 10, S12**). The 'zigzag' runs have impact on the air-sea flux from an earlier date, starting to pull the results away from the SOCAT baseline and toward the 'model truth' already in the late-1990s, while the 'one-latitude' runs do the same about a decade later (**Figs. 10**, **S12**).

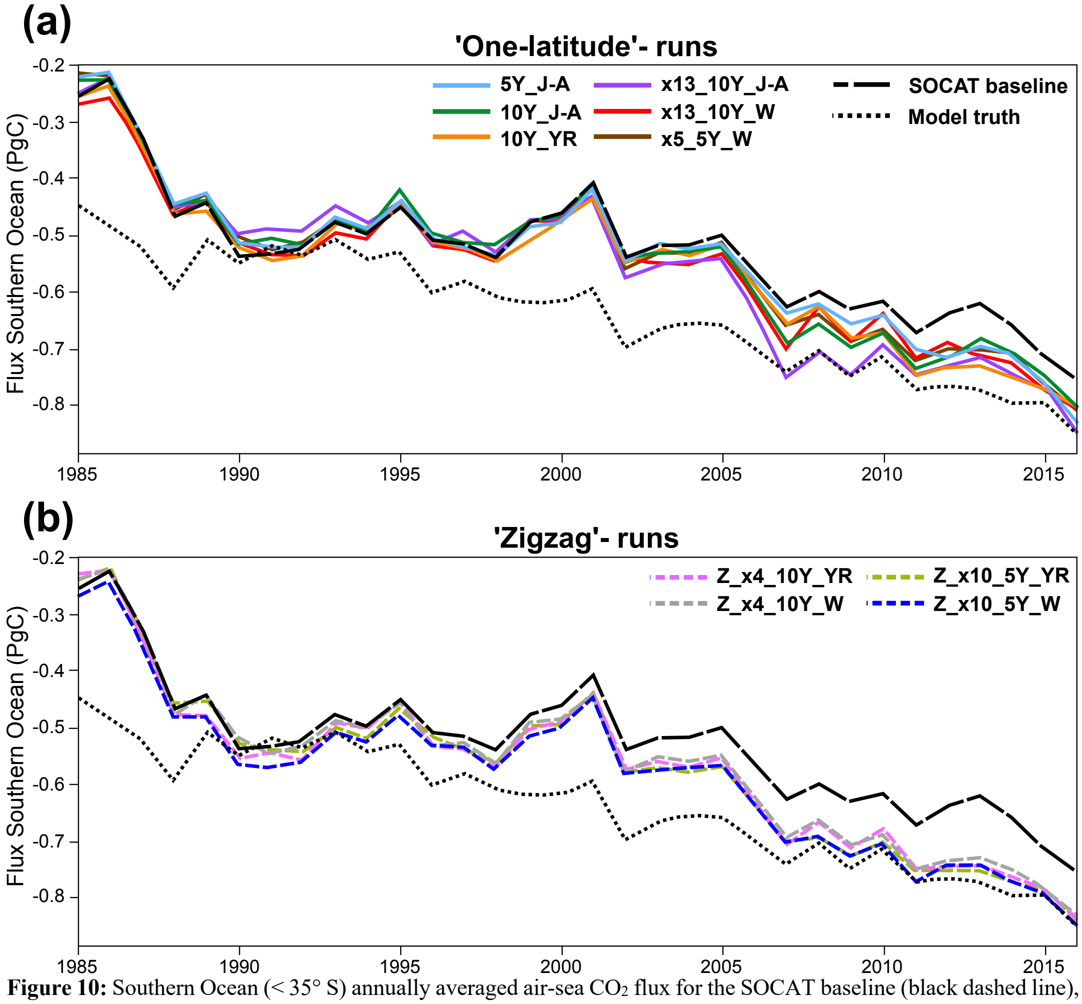

Figure 10: Southern Ocean (< 35° S) annually averaged air-sea CO_2 flux for the SOCAT baseline (black dashed line), 'model truth' (black dotted line) 'one-latitude' runs (**a**; solid lines) and 'zigzag' runs (**b**; dashed lines), averaged over the 75 ensemble members. Compared to the SOCAT baseline, regardless of sampling pattern, the Saildrone USV additions lead to an increased ocean sink. The 'zigzag' runs generate a stronger sink compared to the 'one-latiude' runs, and closely match the 'model truth' for the duration of sample additions.

4. Discussion

We have tested the pCO_2-Residual reconstruction method with the Large Ensemble Testbed (LET) to estimate its fidelity and understand how new samples could increase skill. We find that, regardless of the chosen Saildrone USV sampling pattern, the reduction in both bias and RMSE compared to the SOCAT baseline is most prominent within the Southern Ocean (< 35° S) during the period of which Saildrone USV observations were added (**Figs. 4, 6, 7, 9**). However, it is important to mention that additional Southern Ocean sampling also improves pCO_2 reconstructions globally (**Figs. 5a**, **8a**). Based on our experiments, a combination of factors seems to be important in order to improve both the global and Southern Ocean pCO_2 reconstructions, and include mainly the type of sampling pattern and seasonality of sampling, but also to some extent the number of additional observations. Importantly, increasing the number of observations or duration of sampling (5 vs. 10 years) is not the sole determining factor for improving the reconstructions (**Figs. 5**, **8**). This is best demonstrated by the 'high-sampling'-run 'x13_10Y_J-A' (44,250 observations), which does not provide significantly better reconstructions, or is even outperformed, by runs with 2-18 times less observations, but that cover the full southern hemisphere winter (**Figs. 5**, **6d**, **8**, **9d**). Run 'x13_10Y_J-A' does not include more than a few observations in the month of August, as it follows the temporal pattern of the real-world 'one-latitude' Saildrone USV expedition (**Fig. S1**; Sutton et al., 2021). The 'one-latitude' runs '10Y_J-A' and '10Y_YR' are directly comparable in terms of sample duration, spatial extent and number of observations (**Table 1**), but the latter, which covers all months, always shows lower RMSE and bias (**Figs. 5**, **6d**, **8**, **9d**). These examples attest to the importance of addressing the issue of significant undersampling in the Southern Ocean during the winter season (**Figs. S3a, b**).

Another important comparison is the 'one-latitude'-run 'x5_5Y_W' (5,022 observations) and 'zigzag'-run 'Z_x10_5Y_W' (3,800 observations) that both sample during southern hemisphere winter months over a five-year period (**Table 1**), where the 'zigzag'-run consistently performs better even though it includes fewer observations (**Figs. 5**, **8**). Most of the runs that perform similar to, or outperform, the above-mentioned 'high-sampling'-run 'x13_10Y_J-A' (44,250 observations), sample in a 'zigzag' pattern. Out of all 10 runs, the 'year-round' 'zigzag' runs ('Z_x4_10Y_YR' and 'Z_x10_5Y_YR') are most able to reduce the magnitude of error as shown by the lowest RMSE values (**Figs. 8**, **9d**). A recent study performed similar sampling experiments as shown here, by comparing sampling from different types of autonomous platforms to a SOCAT baseline (Djeutchouang et al., 2022). They emphasized the importance of capturing the significant differences in pCO_2 that exist across meridional gradients during summer and winter months (up to 15 µatm; Djeutchouang et al., 2022). The meridional coverage provided by the 'zigzag' runs could explain why these runs generally outperform the 'one-latitude' runs in our study, and show significant reduction in both RMSE and bias, even though the global pCO_2 data density is raised by as little as 0.01-0.04 %.

The greatest reduction in bias out of all runs is however shown by run 'x13_10Y_W' (**Figs. 5**, **6d**), which represents 'one-latitude' 'high-sampling' (i.e., 25,395 observations) during southern hemisphere winter months only. This sampling strategy seems thus to have a higher ability to reduce the ML model's tendency to overestimate pCO_2 in the Southern Ocean compared to any of the meridional ('zigzag') runs. However, it should be noted that run 'x13_10Y_W' cover areas south of 55° S (**Fig. S2**), and its improvement in bias (and RMSE) is particularly prevalent at such high latitudes (e.g., **Figs. S5**, **S6**, **S8**, **S10**). Whether or not this run is in fact feasible with current or future technology is uncertain as parts of the southernmost tracks cover the Southern Ocean ice zone (**Fig. S13**), and solar radiation for solar-powered platforms and sensors becomes very limited during winter south of 55° S. Furthermore, this particular sampling strategy requires 13 USVs, and thus would be the most costly of the observing scenarios. Although run 'x13_10Y_W' demonstrates the highest reduction in bias out of all runs, the 'zigzag' runs still reduce bias in the Southern Ocean by 44-65 % (vs. 77 % for run 'x13_10Y_W').

Overall, the 'zigzag' runs include significantly fewer observations, require less USVs, collect samples over the same duration, or even half the time as run 'x13_10Y_W', cover areas north of 55°S and within the ice-free zone, and show major improvement in the reconstruction of pCO_2, attested to by reductions in both bias and RMSE. The 'zigzag' runs also closely match both the global and Southern Ocean 'model truth' air-sea CO_2 flux for the duration of sample additions (**Figs. 10**, **S12**). It also appears that the 'zigzag' runs generally have a greater impact on both the pCO_2 reconstruction and the air-sea flux further back in time, starting to deviate from the SOCAT baseline earlier compared to the 'one-latitude' runs (**Figs. 6**, **9**, **10**, **S6**, **S10**, **S11**, **S12**). Even the 'zigzag' scenarios with the least number of USVs (e.g., 'Z_x4_10Y_YR') reduces Southern Ocean reconstruction bias and RMSE by up to 46 % and 13 %, respectively, and could provide a basis for realistic future Southern Ocean pCO_2 sampling campaigns.

The main motivation for improving surface ocean pCO_2 reconstructions is so that we can more accurately estimate the current and future oceanic uptake of anthropogenic carbon. The Southern Ocean is a significant carbon sink, but estimates of the air-sea CO_2 flux diverge substantially in this region (Takahashi et al., 2009; Landschützer et al., 2014, 2015; Rödenbeck et al., 2015; Williams et al., 2017; Gray et al., 2018; Gruber et al., 2019; Bushinsky et al., 2019; Long et al., 2021; Fay and McKinley, 2021; Wu et al., 2022). Southern Ocean estimates incorporating observations from biogeochemical floats have shown a significantly weaker sink compared to those based only on observations from ships (Williams et al., 2017; Gray et al., 2018; Bushinsky et al., 2019). Bushinsky et al. (2019) performed similar sampling experiments as presented here, by comparing ML surface ocean pCO_2 reconstructions based on SOCAT alone vs. additional Southern Ocean floats. They showed that by adding the floats, the Southern Ocean carbon sink (mean of the period of float additions; 2015-2017) decreased (weakened) by 0.4 Pg C yr^{-1}. In contrast, by using a model testbed, we show that adding USVs increased (strengthened) the Southern Ocean and global ocean sink by up to 0.1 Pg C yr^{-1} (**Figs. 10**, **S12**; **Table S3**), which is a significant fraction of the uncertainty in the global ocean carbon sink (0.4 Pg C yr^{-1}; Friedlingstein et al., 2022). Fed with real-world SOCAT data, the global mean air-sea flux estimate from the pCO_2-Residual method is similar to other available products (Bennington et al., 2022a), suggesting that other products may also underestimate the Southern Ocean carbon sink due to the spatio-temporal distribution of SOCAT data. Our experiments suggest that targeted USV observations could reduce this underestimation of the ocean carbon sink.

What else can we learn using the model testbed? The SOCAT baseline demonstrates a weakening of the global and Southern Ocean carbon sink in the 2000s (**Figs. 10**, **S12**), which is in agreement with various data products using real-world SOCAT data (e.g., Gruber et al., 2019; Landschützer et al., 2015; Bushinsky et al., 2019; Bennington et al., 2022; Gloege et al., 2022). Peaks in bias and RMSE coincide in time with the weakening sink (**Figs. 6d, 9d**). As shown by **Figure 10**, this 'low sink' is significantly exaggerated compared to the 'model truth'. To better understand this discrepancy, we performed an additional experiment based on run 'Z_x10_5Y_YR', but assumed sampling every year for the entire testbed period (i.e., 1982-2016). The results from this experiment show a significant reduction in the temporal variability of reconstruction bias; with the additional USV sampling, the reconstructed Southern Ocean air-sea CO_2 flux closely matches the 'model truth' for the entire testbed duration (**Fig. S14**). This suggests that the large decadal variability of air-sea CO_2 fluxes since the 1980s, and the weak anomaly in the Southern Ocean carbon sink in the early 2000s (Le Quéré et al., 2007; Landschützer et al., 2015; Gruber et al., 2019; Bennington et al., 2022a,b; Friedlingstein et al., 2022), may be at least partially attributable to undersampling of the Southern Ocean. We will further explore this issue in future work. Still, this preliminary experiment suggests that interpretations of trends and variability of the global and Southern Ocean carbon sink should be considered with caution.

5. Conclusions

By using the Large Ensemble Testbed (LET), we show that targeted meridional and winter sampling in the Southern Ocean can improve global and Southern Ocean ML surface ocean pCO_2 reconstructions. Significant improvements are possible by raising the global pCO_2 data density by as little as 0.02-0.04 %. Further, we find that this modest amount of additional Saildrone USV sampling increases the global and Southern Ocean air-sea CO_2 flux by up to 0.1 Pg C yr^{-1}, 25 % of the uncertainty in the ocean carbon sink. Our findings are consistent with previous studies suggesting that additional observations during southern hemisphere winter months and covering meridional gradients can reduce uncertainties and biases in the reconstructions (Lenton et al., 2006; Monteiro et al., 2010; Djeutchouang et al., 2022; Mackay et al., 2022). As opposed to other autonomous platform approaches, Saildrone USVs obtain in situ pCO_2 observations with uncertainties equivalent to the highest-quality observations collected by research ships (± 2 µatm; Sabine et al., 2020; Sutton et al., 2021), and can operate at a high speed so that the spatial extent and seasonal cycle of meridional gradients can be covered. The approach of combining high-accuracy Saildrone USV and SOCAT observations represents thus a promising solution to improve future surface ocean pCO_2 reconstructions and the accuracy of the ocean carbon sink. Lastly, we show that the large variability in bias, and the weakening of the global and Southern Ocean carbon sink in the 2000s, may be partially an artefact of Southern Ocean undersampling.

Code availability

Data analysis scripts will be made available in a GitHub repository upon publication.

Data availability

The Large Ensemble Testbed is publicly available at https://figshare.com/collections/Large_ensemble_pCO2_testbed/4568555.

Author contribution

THH, GAM and AJS designed the experiments, and THH performed the simulations. THH, ARF and LG developed the code. THH and ARF calculated the air-sea fluxes. THH prepared the manuscript with contributions from all co-authors.

Competing interests

The authors declare that they have no conflict of interest.

Acknowledgements

We acknowledge funding from NOAA through the Climate Observations and Monitoring Program (Award #NA20OAR4310340) and from NSF through the LEAP STC (Award #2019625). This is PMEL contribution 5549. We would also like to acknowledge and thank Julius Busecke and Devan Samant for providing technical support.

References

Bakker, D. C. E., Pfeil, B., Landa, C. S., Metzl, N., O'Brien, K. M., Olsen, A., Smith, K., Cosca, C., Harasawa, S., Jones, S. D., Nakaoka, S., Nojiri, Y., Schuster, U., Steinhoff, T., Sweeney, C., Takahashi, T., Tilbrook, B., Wada, C., Wanninkhof, R., Alin, S. R., Balestrini, C. F., Barbero, L., Bates, N. R., Bianchi, A. A., Bonou, F., Boutin, J., Bozec, Y., Burger, E. F., Cai, W.-J., Castle, R. D., Chen, L., Chierici, M., Currie, K., Evans, W., Featherstone, C., Feely, R. A., Fransson, A., Goyet, C., Greenwood, N., Gregor, L., Hankin, S., Hardman-Mountford, N. J., Harlay, J., Hauck, J., Hoppema, M., Humphreys, M. P., Hunt, C. W., Huss, B., Ibánhez, J. S. P., Johannessen, T., Keeling, R., Kitidis, V., Körtzinger, A., Kozyr, A., Krasakopoulou, E., Kuwata, A., Landschützer, P., Lauvset, S. K., Lefèvre, N., Lo Monaco, C., Manke, A., Mathis, J. T., Merlivat, L., Millero, F. J., Monteiro, P. M. S., Munro, D. R., Murata, A., Newberger, T., Omar, A. M., Ono, T., Paterson, K., Pearce, D., Pierrot, D., Robbins, L. L., Saito, S., Salisbury, J., Schlitzer, R., Schneider, B., Schweitzer, R., Sieger, R., Skjelvan, I., Sullivan, K. F., Sutherland, S. C., Sutton, A. J., Tadokoro, K., Telszewski, M., Tuma, M., van Heuven, S. M. A. C., Vandemark, D., Ward, B., Watson, A. J., and Xu, S.: A multi-decade record of high-quality *f*CO_2 data in version 3 of the Surface Ocean

CO_2 Atlas (SOCAT), Earth System Science Data, 8, 383–413, https://doi.org/10.5194/essd-8-383-2016, 2016.

Bennington, V., Galjanic, T., and McKinley, G. A.: Explicit Physical Knowledge in Machine Learning for Ocean Carbon Flux Reconstruction: The pCO_2-Residual Method, Journal of Advances in Modeling Earth Systems, 14(10), https://doi.org/10.1029/2021ms002960, 2022a.

Bennington, V., Gloege, L., and McKinley, G. A.: Variability in the global ocean carbon sink from 1959 to 2020 by correcting models with observations, Geophysical Research Letters, 49(14), https://doi.org/10.1029/2022GL098632, (2022b).

Bushinsky, S. M., Landschützer, P., Rödenbeck, C., Gray, A. R., Baker, D., Mazloff, M. R., Resplandy, L., Johnson, K. S., and Sarmiento, J. L.: Reassessing Southern Ocean air-sea CO_2 flux estimates with the addition of biogeochemical float observations, Global Biogeochemical Cycles, *33*(11), 1370-1388, https://doi.org/10.1029/2019GB006176, 2019.

Chen, T., and Guestrin, C.: Xgboost: A scalable tree boosting system, In: Proceedings of the 22nd ACM SIGKDD international conference on knowledge discovery and data mining (pp. 785-794), https://doi.org/10.1145/2939672.2939785, 2016.

Deser, C., Phillips. A., Bourdette, V., and Teng. H.: Uncertainty in climate change projections: the role of internal variability, Climate Dynamics, 38, 527-546, https://doi.org/10.1007/s00382-010-0977-x, 2012

Djeutchouang, L. M., Chang, N., Gregor, L., Vichi, M., and Monteiro, P. M. S.: The sensitivity of *p*CO_2 reconstructions to sampling scales across a Southern Ocean sub-domain: a semi-idealized ocean sampling simulation approach, Biogeosciences, 19, 4171-4195, https://doi.org/10.5194/bg-19-4171-2022, 2022

Fay, A. R., Lovenduski, N. S., McKinley, G. A., Munro, D. R., Sweeney, C., Gray, A. R., Landschützer, P., Stephens, B. B., Takahashi, T., and Williams, N.: Utilizing the Drake Passage Time-series to understand variability and change in subpolar Southern Ocean pCO_2, Biogeosciences, 15(12), 3841-3855, https://doi.org/10.5194/bg-15-3841-2018, 2018.

Fay, A. R., and McKinley, G. A.: Observed regional fluxes to constrain modeled estimates of the ocean carbon sink, Geophysical Research Letters, 48(20), https://doi.org/10.1029/2021GL095325, 2021

Friedlingstein, P., Jones, M. W., O'Sullivan, M., Andrew, R. M., Bakker, D. C., Hauck, J., Le Quéré, C., Peters, G. P., Peters, W., Pongratz, J., Sitch, S., Canadell, J. G., Ciais, P., Jackson, R. B., Alin, S. R., Anthoni, P., Bates, N. R., Becker, M., Bellouin, N., Bopp, L., Chau, T. T. T., Chevallier, F., Chini, L. P., Cronin, M., Currie, K. I., Decharme, B., Djeutchouang, L., Dou, X., Evans, W., Feely, R. A., Feng, L., Gasser, T., Gilfillan, D., Gkritzalis, T., Grassi, G., Gregor, L., Gruber, N., Gürses, Ö., Harris, I., Houghton, R. A., Hurtt, C. C., Iida, Y., Ilyina, T., Luijkx, I. T., Jain, A. K., Jones, S. D., Kato, E., Kennedy, D., Goldewijk, K. K., Knauer, J., Korsbakken, J. A., Körtzinger, A., Landschützer, P., Lauvset, S. K., Lefèvre, N., Lienert, S., Liu, J., Marland, G., McGuire, P. C., Melton, J. R., Munro, D. R., Nabel, J. E. M. S., Nakaoka, S-I., Niwa, Y., Ono, T., Pierrot, D., Poulter, B., Rehder, G., Resplandy, L., Robertson, E., Rödenbeck, C., Rosan, T. M., Schwinger, J., Schwingshackl, C., Séférian, R., Sutton, A. J., Sweeney, C., Tanhua, T., Tans, P. P., Tian, H., Tilbrook, B., Tubiello, F., Werf, G. V. D., Vuichard, N., Wada, C., Wanninkhof, R., Watson, A., Willis, D., Wiltshire, A. J., Yuan, W., Yue, C., Yue, X., Zaehle, S., and Zeng, J.: Global carbon budget 2021, Earth System Science Data, 14(4), 1917-2005, https://doi.org/10.5194/essd-14-1917-2022, 2022

Fyfe, J. C., Derksen, C., Mudryk, L., Flato, G. M., Santer, B. D., Swart, N. C., Molotch, N. P., Zhang, X., Wan, H., Arora, V. K., Scinocca, J., and Jiao, Y.: Large near-term projected snowpack loss over the western United States, Nature communications, 8(1), 14996, https://doi.org/10.1038/ncomms14996, 2017.

Gloege, L., McKinley, G. A., Landschützer, P., Fay, A. R., Frolicher, T. L., and Fyfe, J. C.: Quantifying Errors in Observationally Based Estimates of Ocean Carbon Sink Variability, Global Biogeochemical Cycles, 35(4), https://doi.org/10.1029/2020gb006788, 2021.

Gloege, L., Yan, M., Zheng, T. and McKinley, G. A.: Improved quantification of ocean carbon uptake by using machine learning to merge global models and pCO_2 data, Journal of Advances in Modeling Earth Systems, 14(2), https://doi.org/10.1029/2021MS002620, 2022.

Good, S. A., Martin, M., and Rayner, N. A.: EN4: Quality controlled ocean temperature and salinity profiles and monthly objective analyses with uncertainty estimates, Journal of Geophysical Research Oceans, 118(12), 6704-6717, https://doi.org/10.1002/2013JC009067, 2013.

Gray, A. R., Johnson, K. S., Bushinsky, S. M., Riser, S. C., Russell, J. L., Talley, L. D., Wanninkhof, R., Williams, N. L., and Sarmiento, J. L.: Autonomous biogeochemical floats detect significant carbon dioxide outgassing in the high-latitude Southern Ocean, Geophysical Research Letters, 45(17), 9049-9057, https://doi.org/10.1029/2018GL078013, 2018.

Gregor, L., Lebehot, A. D., Kok, S., and Monteiro, P. M. S.: A comparative assessment of the uncertainties of global surface ocean CO_2 estimates using a machine-learning ensemble (CSIR-ML6 version 2019a) – have we hit the wall?, Geoscientific Model Development, 12, 5113-5136, https://doi.org/10.5194/gmd-12-5113-2019, 2019.

Gregor, L. and Fay, A. R.: Air-sea CO_2 fluxes for surface pCO_2 data products using a standardized approach, Zenodo [code], https://doi.org/10.5281/zenodo.5482547, 2021.

Gruber, N., Landschützer, P., and Lovenduski, N. S.: The variable Southern Ocean carbon sink, The Annual Review of Marine Science, 11, 159-86, https://doi.org/10.1146/annurev-marine-121916-063407, 2019.

Kay, J. E., Deser, C., Phillips, A., Mai, A., Hannay, C., Strand, G., Arblaster, J. M., Bates, S. C., Danabasoglu, G., Edwards, J., Holland, M., Kuschner, P., Lamarque, J-F., Lawrence, D., Lindsay, K., Middelton, A., Munoz, E., Nealse, R., Oleson, K., Polvani, L., and Vertenstein, M.: The Community Earth System Model (CESM) large ensemble project: A community resource for studying climate change in the presence of internal climate variability, Bulletin of the American Meteorological Society, 96(8), 1333-1349, https://doi.org/10.1175/BAMS-D-13-00255, 2015.

Khatiwala, S., Primeau, F., and Hall., T.: Reconstruction of the history of anthropogenic CO2 concentrations in the ocean, Nature, 462(7271), 346-349, https://doi.org/10.1038/nature08526, 2009.

Landschützer, P., Gruber, N., Bakker, D. C. E., and Schuster, U.: Recent variability of the global ocean carbon sink, Global Biogeochemical Cycles, 28(9), 927-949, https://doi.org/10.1002/2014GB004853, 2014.

Landschützer, P., Gruber, N., Haumann, F. A., Rödenbeck, C., Bakker, D. C. E., Van Heuven, S., Hoppema, M., Metzl, N., Sweeney, C., Takahashi, T., Brook, B., and Wanninkhof, R.: The reinvigoration of the Southern Ocean carbon sink, Science, 349(6253), 1221-1224. https://doi.org/10.1126/science.aab2620, 2015.

Landschützer, P., Tanhua, T., Behncke, J., and Keppler, L.: Sailing through the Southern Ocean seas of air-sea CO_2 flux uncertainty, Philosophical Transactions of the Royal Society A, 381, https://doi.org/10.1098/rsta.2022.0064, 2023.

Lenton, A. B., Matear, R. J., and Tilbrook, B.: Design of an observational strategy for quantifying the Southern Ocean uptake of CO_2, Global Biogeochemical Cycles, 20, 1-11. https://doi.org/10.1029/2005GB002620, 2006.

Lenton, A. B., Tilbrook, B., Law, R. M., Bakker, D. C. E., Doney, S. C., Gruber, N., Ishii, M., Hoppema, M., Lovenduski, N. S., Matear, R. J., McNeil. B. I., Metzl, N., Mikaloff Fletcher, S. E., Monteiro, P. M. S., Rödenbeck, C., Sweeney, C., and Takahashi, T.: Sea-air CO_2 fluxes in the Southern Ocean for the period 1990-2009, Biogeosciences, 10, 4037-4054, https://doi.org/10.5194/bg-10-4037-2013, 2013.

Le Quéré, C., Rödenbeck, C., Buitenhuis, E. T., Conway, T. J., Lagenfelds, R., Gomez, A., Labuschagne C., Ramonet, M., Nakazawa, T., Metzl, N., Gillett, N., and Heimann, M.: Saturation of the Southern Ocean CO2 sink due to recent climate change, Science, 316(5832), 1735-1738, https://doi.org/10.1126/science.1136188, 2007.

Long, M. C., Stephens, B. B., McKain, K., Sweeney, C., Keeling, R. F., Kort, E. A., Morgan, E. J., Bent, J. D., Chandra, N., Chevallier, F., Commane, R., Daube, B. C., Krummel, P. B., Loh, Z., Luijkx, I. T., Munro, D., Patra, P., Peters, W., Ramonet, M., Rödenbeck, C., Stavert, A., Tans, P., and Wofsy, S. C.: Strong Southern Ocean carbon uptake evident in airborne observations, Science, 374(6572), 1275-1280, https://doi.org/10.1126/science.abi4355, 2021.

Mackay, N., and Watson, A.: Winter air-sea CO_2 fluxes constructed from summer observations of the polar Southern Ocean suggest weak outgassing, Journal of Geophysical Research: Oceans, 126(5), e2020JC016600, https://doi.org/10.1029/2020JC016600, 2021.

Mackay, N., Watson, A., Suntharalingam, P., Chen, Z., and Rödenbeck, C.: Improved winter data coverage of the Southern Ocean CO_2 sink from extrapolation of summertime observations, Communications Earth & Environment, 3, 265, https://doi.org/10.1038/s43247-022-00592-6, 2022.

McKinley, G. A., Fay, A. R., Eddebbar, Y. A., Gloege, L., and Lovenduski, N. S.: External forcing explains recent decadal variability of the ocean carbon sink, AGU Advances, 1(2), e2019AV000149, https://doi.org/10.1029/2019AV000149, 2020.

Mongwe, N. P., Vichi, M., and Monteiro, P. M. S.: The seasonal cycle of pCO$_2$ and CO_2 fluxes in the Southern Ocean: diagnosing anomalies in CMIP5 Earth system models, Biogeosciences, 15(9), 2851-2872, https://doi.org/10.5194/bg-15-2851-2018, 2018.

Monteiro, P. M. S., Gregor, L., Lévy, M., Maenner, S., Sabine, C. L., and Swart, S.: Intraseasonal variability linked to sampling alias in air-sea CO_2 fluxes in the Southern Ocean, Geophysical Research Letters, 42(20), 8507-8514, https://doi.org/10.1002/2015GL066009, 2015.

Rodgers, K. B., Lin, J., and Frölicher, T. L.: Emergence of multiple ocean ecosystem drivers in a large ensemble suite with an Earth system model, Biogeosciences, 12(11), 3301-3320. https://doi.org/10.5194/bg-12-3301-2015, 2015.

Rödenbeck, C. Bakker, D. C. E., Gruber, N., Iida, Y., Jacobson, A. R., Jones, S., Landschützer, P., Metzl, N., Nakaoka, S., Olsen, A., Park, G.-H., Peylin, P., Rodgers, K. B., Sasse T. P., Schuster, U., Shutler, J. D., Valsala, V., Wannikkhof, R., and Zeng, J.: Data-based estimates of the ocean carbon sink variability – first results of the Surface Ocean pCO$_2$ Mapping intercomparison (SOCOM), Biogeosciences, 12, 7251-7278. https://doi.org/10.5194/bg-12-7251-2015, 2015.

Sabine, C., Sutton, A., McCabe, K., Lawrence-Slavas, N., Alin, S, Feely, R., Jenkins, R., Maenner, S., Meinig, C., Thomas, J., van Ooijen, E., Passmore, A., and Tilbrook, B.: Evaluation of a new carbon dioxide system for autonomous surface vehicles, Journal of Atmospheric and Oceaenic Technology, 37(8), 1305-1317, https://doi.org/10.1175/JTECH-D-20-0010.1, 2020.

Stamell, J., Rustagi, R. R., Gloege, L., and McKinley, G. A.: Strengths and weaknesses of three Machine Learning methods for pCO_2 interpolation, Geoscientific Model Development Discussions[preprint], doi:10.5194/gmd-2020-311, 22 October 2020.

Sutton, A. J., Williams, N. L., and Tilbrook, B.: Constraining Southern Ocean CO_2 flux uncertainty using uncrewed surface vehicle observations, Geophysical Research Letters, 48(3), e2020GL091748, https://doi.org/10.1029/2020GL091748, 2021.

Takahashi, T., Olafsson, J., Goddard, J. G., Chipman, D. W., and Sutherland, S. C.: Seasonal variation of CO2 and nutrients in the high-latitude surface oceans: A comparative study, Global Biogeochemical Cycles, 7(4), 843-878, https://doi.org/10.1029/93GB02263, 1993.

Takahashi, T., Sutherland, S. C., Wanninkhof, R., Sweeney, C., Feely, R. A., Chipman, D. W., Hales, B., Friederich, G., Chavez, F., Sabine, C., Watson, A., Bakker, D. C. E., Schuster, U., Metzl, N., Yoshikawa-Inoue, H., Ishii, M., Midorikawa, T., Nojiri, Y., Körtzinger, A., Steinhoff, T., Hoppema, M., Olafsson, J., Arnarson, T. S., Tilbrook, B., Johannessen, T., Olsen, A., Bellerby, R., Wong, C. S., Delille, B., Bates, N. R., and de Baar, H. J. W.: Climatological mean and decadal change in surface ocean pCO_2, and net sea-air CO_2 flux over the global oceans, Deep Sea Research Part II: Topical Studies in Oceanography, 56(8-10), 554-557, https://doi.org/10.1016/j.dsr2.2008.12.009, 2009.

Toms, B. A., Barnes, E. A., and Ebert-Uphoff, I.: Physically interpretable neural networks for the geosciences: Applications to earth system variability, Journal of Advances in Modeling Earth Systems, 12(9), e2019MS002002, https://doi.org/10.1029/2019MS002002, 2020.

Williams, N. L., Juranek, L. W., Feely, R. A., Johnson, K. S., Sarmiento, J. L., Talley, L. D., Dickson, A. G., Gray, A. R., Wannikhof, R., Russell, J. L., Riser, S. C., and Takeshita, Y.: Calculating surface ocean pCO_2 from biogeochemical Argo floats equipped with pH: An uncertainty analysis, Global Biogeochemical Cycles, 31(3), 591-604, https://doi.org/10.1002/2016GB005541, 2017.

Wu, Y., Bakker, D. C. E., Achterberg, E. P., Silva, A. N., Pickup D. P., Li, X., Hartman, S., Stappard, D., Qi, D., and Tyrrell, T.: Integrated analysis of carbon dioxide and oxygen concentrations as a quality control of ocean float data, Communications Earth & Environment, 3, 92, https://doi.org/10.1038/s43247-022-00421-w, 2022.